IEEE Access
Multidisciplinary | Rapid Review | Open Access Journal

Received September 20, 2020, accepted September 27, 2020, date of publication October 6, 2020, date of current version October 21, 2020.

Digital Object Identifier 10.1109/ACCESS.2020.3029095

Fuzzy-Based Super-Twisting Sliding Mode Stabilization Control for Under-Actuated Rotary Inverted Pendulum Systems

NGO PHONG NGUYEN[1], HYONDONG OH[1], (Senior Member, IEEE), YOONSOO KIM[2], (Member, IEEE), JUN MOON[3], (Senior Member, IEEE), JUN YANG[4], (Senior Member, IEEE), AND WEN-HUA CHEN[4], (Fellow, IEEE)

[1]School of Mechanical, Aerospace and Nuclear Engineering, Ulsan National Institute of Science and Technology (UNIST), Ulsan 44919, South Korea
[2]Department of Aerospace and Software Engineering, Gyeongsang National University, Jinju 52828, South Korea
[3]Department of Electrical Engineering, Hanyang University, Seoul 04763, South Korea
[4]Department of Aeronautical and Automotive Engineering, Loughborough University, Loughborough LE11 3TU, U.K.

Corresponding authors: Hyondong Oh (h.oh@unist.ac.kr) and Jun Moon (junmoon@hanyang.ac.kr)

This work was supported in part by the National Research Foundation of Korea (NRF) grant funded by the Ministry of Science and ICT under Grant NRF-2017R1A5A1015311, and in part by the Basic Science Research Program through the National Research Foundation of Korea (NRF) grant funded by the Ministry of Education under Grant 2020R1A6A1A03040570.

ABSTRACT This paper considers the stabilization problem for under-actuated rotary inverted pendulum systems (RotIPS) via a fuzzy-based continuous sliding mode control approach. Various sliding mode control (SMC) methods have been proposed for stabilizing the under-actuated RotIPS. However, there are two main drawbacks of these SMC approaches. First, the existing SMCs have a discontinuous structure; therefore, their control systems suffer from the chattering problem. Second, a complete proof of closed-loop system stability has not been provided. To address these two limitations, we propose a fuzzy-based (continuous) super-twisting stabilization algorithm (FBSTSA) for the under-actuated RotIPS. We first introduce a new sliding surface, which is designed to resolve the under-actuation problem, by combining the fully-actuated (rotary arm) and the under-actuated (pendulum) variables to define one sliding surface. Then, together with the proposed sliding surface, we develop the FBSTSA, where the corresponding control gains are adjusted based on a fuzzy logic scheme. Note that the proposed FBSTSA is continuous owing to the modified super-twisting approach, which can reduce the chattering and enhance the control performance. With the proposed FBSTSA, we show that the sliding variable can reach zero in finite time and then the closed-loop system state converges to zero asymptotically. Various simulation and experimental results are provided to demonstrate the effectiveness of the proposed FBSTSA. In particular, (i) compared with the existing SMC approaches, chattering is alleviated and better stabilization is achieved; and (ii) the robustness of the closed-loop system (with the proposed FBSTSA) is guaranteed under system uncertainties and external disturbances.

INDEX TERMS Asymptotic stability, finite-time stability, fuzzy-based super-twisting sliding mode control, rotary inverted pendulum system, stabilization control.

I. INTRODUCTION

Rotary inverted pendulums were first developed by Furuta and his colleagues at the Tokyo Institute of Science and Technology [1], [2]. The Furuta pendulum comprises a rotary arm that rotates in the horizontal plane and a pendulum link connected to the end of the rotary arm, which is free to rotate in the vertical plane [1], [2] (see Fig. 1). The rotary inverted pendulum belongs to a class of two-degree-of-freedom under-actuated system since its motion is composed of the rotation of the arm and the pendulum; however, only the arm is subjected to the control input torque [1], [2].

Concerning the stabilization task of the under-actuated RotIPS, it is a common-but-challenging objective in control theory. The RotIPS is a popular control benchmark because its shape and dynamic in the upright position can mimic many

The associate editor coordinating the review of this manuscript and approving it for publication was Hao Luo.

FIGURE 1. The Quanser rotary inverted pendulum. Image courtesy of Quanser Inc. [24].

real world applications, such as Segways and rocket systems; see [1], [2] and the references therein. In addition, the RotIPS is also presented in other fields of industrial engineering systems, such as flexible systems, locomotive systems, and marine systems [1], [2]. The challenges in controlling the RotIPS arise because the dynamic model governing the system is strongly coupled and nonlinear, and the equilibrium point in the upright position is unstable.

Various kinds of control approaches have been proposed to address these challenges, including linear control methods [3]–[5], generic nonlinear control approaches [6], [7], adaptive control methods [8], [9], fuzzy control techniques [10], [11], and sliding mode control approaches [12]–[15]. Interested readers are referred to [1], [2] for more details about the linear and the nonlinear stabilization controllers for the RotIPS. Among the methods described in [1], [2], sliding mode control (SMC) is considered as an effective control approach for stabilizing the RotIPS because of its ease of implementation and rapid transient response [12]–[15].

The SMC design is typically divided into two stages. In the first stage, a sliding surface on which sliding motion occurs is defined. Then, a finite-time (discontinuous/continuous) control law must be proposed to force the system states converging to the desired sliding surface. Once the sliding motion is achieved, the stability of the closed-loop system is ensured [16]–[18]. We mention that the SMC approach has been employed successfully for different fully-actuated systems. Interested readers are referred to [19]–[21] for various applications of the (discontinuous/continuous) SMC to fully-actuated nonlinear systems. However, it should be pointed out again that the RotIPS is an under-actuated, open-loop unstable, and highly nonlinear complex dynamic system. Hence, it is difficult to apply these SMCs directly to the stabilization control of the under-actuated RotIPS. In particular, one of the most challenging problems, inhibiting the application of the SMC to the RotIPS, is defining a legitimate sliding surface. Specifically, a proper sliding surface must be designed in such a way that the stability of the fully-actuated (rotary arm) and the under-actuated (pendulum) state variables can be achieved simultaneously in the sliding phase. This is owed to the inherent under-actuated nature of the RotIPS, in contrast to fully-actuated systems. Generally, it is straightforward to develop nonlinear (discontinuous/continuous) SMC laws safeguarding that the sliding variable converges to zero in finite time. However, a thorough mathematical examination is required to show the stability of the fully-actuated (rotary arm) and the under-actuated (pendulum) state variables in the sliding phase.

A series of SMCs has been developed for stabilizing the under-actuated RotIPS, which can be found in [12]–[15], where different sliding surfaces were utilized. In [12], a decoupled SMC for the RotIPS was proposed. The authors first decoupled the dynamics of the RotIPS into two second-order subsystems. Then, a *discontinuous* SMC was designed to ensure the finite-time reachability of the sliding surface. Moreover, the authors in [13] developed a *discontinuous* nonlinear SMC for the Furuta pendulum. The proposed controller was shown to have better control performance than the linearization feedback controller in terms of convergence rate and control accuracy. In addition, in [14], a nonlinear stabilization model-based controller was developed for the under-actuated RotIPS. To describe the model, the authors first derived two third-order differential equations. Then, a *discontinuous* SMC-based stabilization controller was proposed to achieve the control purpose. Experimental results indicated a better control performance of the proposed controller, compared with that of the linear quadratic controller. Recently, the authors in [15] proposed a dynamic inversion-based SMC for the RotIPS. The dynamic model of the RotIPS was first linearized around the unstable equilibrium point. Then, the equivalent control law in the proposed framework was designed using the Moore-Penrose generalized inversion method, and the switching control part was developed based on the *discontinuous* SMC.

From the control perspective, there are *two main drawbacks* of these SMC methods:

(D-1) the existing SMC approaches [12]–[15] have discontinuous variable structures; therefore, their control systems suffer from the chattering problem. For a practical system, the chattering problem might degrade the control performance and cause potential damage to the actuators;

(D-2) a complete proof for the stability of the under-actuated RotIPS has not been provided in [12]–[15]. Only the system stability analysis in the reaching phase was presented. In other words, the convergence of the system state variables during the sliding phase was not analyzed. From the control aspect, the system stability during the sliding phase is also important since the instability of the closed-loop system during the sliding phase may lead to undesirable

motion of the RotIPS, which could degrade the entire system performance.

In this paper, we address both (D-1) and (D-2) for the under-actuated RotIPS. In particular, we propose a fuzzy-based (continuous) super-twisting stabilization algorithm (FBSTSA) for the under-actuated RotIPS. We present the main contributions of this paper in the next subsection, which is followed by a detailed comparison of the proposed FBSTSA with the existing SMC approaches.

MAIN CONTRIBUTIONS

The main contributions can be summarized as follows:

(i) we propose a fuzzy-based (continuous) super-twisting stabilization algorithm (FBSTSA) for the under-actuated RotIPS. As part of the FBSTSA, a new sliding surface is designed to resolve the under-actuation problem. This surface is defined by combining the fully-actuated (rotary arm) and the under-actuated (pendulum) variables. The corresponding super-twisting control gains in the proposed FBSTSA are adjusted based on a fuzzy logic scheme, which can alleviate the chattering phenomenon and enhance the control performance. Note that this feature overcomes the first limitation (see the statement in (D-1));

(ii) the stability of the under-actuated RotIPS under the proposed FBSTSA in both the reaching and the sliding phases is addressed. We show that the sliding variable can reach zero in finite time in the reaching phase, and then the closed-loop system state converges to zero asymptotically in the sliding phase. This contribution resolves the second limitation (see the statement in (D-2)); and

(iii) various simulation and experimental results are provided to demonstrate the effectiveness of the proposed FBSTSA. In particular, (i) compared with the existing SMC approaches, chattering is alleviated and better stabilization is achieved; and (ii) the robustness of the closed-loop system (with the proposed FBSTSA) is guaranteed under system uncertainties and sudden external disturbances.

To the best of our knowledge, our paper is the first to consider fuzzy-based super-twisting sliding mode stabilization control for the under-actuated RotIPS, where the stability of the closed-loop system is addressed in both the reaching and the sliding phases.

COMPARISON

For the stabilization control problem of the under-actuated RotIPS, our paper can be viewed as an extension of [12]–[15], [22], [23]:

(i) compared with [12]–[15], our paper shows the stability of the closed-loop system in the reaching phase, as well as in the sliding phase;

(ii) we consider a continuous fuzzy-based super-twisting control law, whereas [12]–[15] used the traditional discontinuous) first-order SMC approach;

(iii) we generalize the results of the super-twisting algorithm (STA) in [22], [23] to the case of under-actuated systems with fuzzy-based gains; and

(iv) compared with the proposed adaptive gains in [23], our proposed fuzzy-based gains ensure the finite-time convergence to zero rather than to a small region around zero of the sliding variable.

It should be noted that generalizations of [12]–[15], [22], [23] are not that as straightforward as they appear owing to the under-actuated structure of the RotIPS. The features of the SMCs in [12]–[15], [22], [23] and the proposed FBSTSA are listed in Table 1.

TABLE 1. Features of SMC, STA, and proposed FBSTSA.

	Controller	Reaching stability	Sliding stability
SMC [12]–[15]	Discontinuous	Finite-time	N/A
STA [22], [23]	Continuous	Finite-time	N/A
Proposed FBSTSA	Continuous	Finite-time	Asymptotic

The remainder of this paper is organized as follows. Section II presents the problem formulation in which the dynamic model of the under-actuated RotIPS and the control objective are given. In Section III, the main results of this paper are presented, where the FBSTSA is proposed and the closed-loop system stability is analyzed. The simulation and experimental results are provided in Sections IV and V, respectively. Concluding remarks and future works are presented in Section VI.

II. PROBLEM FORMULATION

In this section, we first derive the dynamic model of the under-actuated RotIPS. Then, we state the control objective of our paper.

A. DYNAMIC MODEL OF THE ROTARY INVERTED PENDULUM SYSTEM

In this paper, we use the Quanser rotary inverted pendulum module.[1] As shown in Fig. 1, the pendulum section is connected at the end of the rotary arm section. The simplified free body diagram of the mechanical components is illustrated in Fig. 2. In the figure, the arm has a mass of m_r, a total length of L_r, and a moment of inertia of J_r. The pendulum attached to the arm has a mass of m_p, a total length of L_p, and a moment of inertia about its center of mass of J_p. In addition, the positive angular rotation is counter-clockwise (CCW).

By using the Euler-Lagrange method, the nonlinear dynamic model of the RotIPS can be derived as follows [24]:

$$\left(\overline{J}_r + \frac{1}{4}m_p L_p^2 \sin^2(\alpha)\right)\ddot{\theta} - \frac{1}{2}m_p L_p L_r \cos(\alpha)\ddot{\alpha}$$

[1] https://www.quanser.com/products/rotary-inverted-pendulum/

$$+\frac{1}{2}m_pL_p^2\sin(\alpha)\cos(\alpha)\dot{\theta}\dot{\alpha}+\frac{1}{2}m_pL_pL_r\sin(\alpha)\dot{\alpha}^2=\tau$$
$$\left(J_p+\frac{1}{4}m_pL_p^2\right)\ddot{\alpha}-\frac{1}{2}m_pL_pL_r\cos(\alpha)\ddot{\theta}$$
$$-\frac{1}{4}m_pL_p^2\sin(\alpha)\cos(\alpha)\dot{\theta}^2-\frac{1}{2}m_pL_pg\sin(\alpha)=0, \quad (1)$$

where $\bar{J}_r := m_pL_r^2 + J_r$. The definitions of the system parameters are given in Table 2. A detailed derivation of (1) can be found in [24].

TABLE 2. The parameters of the under-actuated RotIPS.

Parameters	Description	Unit
m_p	Mass of the pendulum	kg
L_p	Total length of the pendulum	m
J_p	Moment of inertia of the pendulum	kg.m^2
m_r	Mass of the rotary arm	kg
L_r	Total length of the rotary arm	m
J_r	Moment of inertia of the rotary arm	kg.m^2
g	Gravity acceleration constant	m/s^2
θ	Arm angle	rad
α	Pendulum angle	rad
τ	Control input torque	N.m

The rotary inverted pendulum equations of (1) can be rewritten as follows:

$$\ddot{\theta} = f_\theta(\alpha,\dot{\alpha},\dot{\theta}) + g_\theta(\alpha)\tau$$
$$\ddot{\alpha} = f_\alpha(\alpha,\dot{\alpha},\dot{\theta}) + g_\alpha(\alpha)\tau, \quad (2)$$

where

$$f_\theta(\alpha,\dot{\alpha},\dot{\theta}) := \frac{4J_\alpha}{J_\theta(\alpha)}\Big[\dot{\theta}\Big(-\frac{1}{2}m_pL_p^2\sin(\alpha)\cos(\alpha)\dot{\alpha}$$
$$+\frac{1}{8J_\alpha}m_p^2L_p^3L_r\sin(\alpha)\cos^2(\alpha)\dot{\theta}\Big)$$
$$-\frac{1}{2}m_pL_pL_r\sin(\alpha)\dot{\alpha}^2$$
$$+\frac{1}{4J_\alpha}m_p^2L_p^2L_rg\sin(\alpha)\cos(\alpha)\Big]$$
$$f_\alpha(\alpha,\dot{\alpha},\dot{\theta}) := \frac{1}{J_\theta(\alpha)}m_pL_pL_r\cos(\alpha)\Big(-m_pL_pL_r\sin(\alpha)\dot{\alpha}^2$$
$$-m_pL_p^2\sin(\alpha)\cos(\alpha)\dot{\theta}\dot{\alpha}\Big)$$
$$+\left(4\bar{J}_r+m_pL_p^2\sin^2(\alpha)\right)$$
$$\times\Big[\frac{1}{4J_\theta(\alpha)}m_pL_p^2\sin(\alpha)\cos(\alpha)\dot{\theta}^2$$
$$+\frac{1}{2J_\theta(\alpha)}m_pL_pg\sin(\alpha)\Big]$$
$$g_\theta(\alpha) := \frac{4J_\alpha}{J_\theta(\alpha)},\ g_\alpha(\alpha) := \frac{2}{J_\theta(\alpha)}m_pL_pL_r\cos(\alpha)$$
$$J_\theta(\alpha) := 4J_\alpha\bar{J}_r + J_\alpha m_pL_p^2\sin^2(\alpha) - m_p^2L_p^2L_r^2\cos^2\alpha$$
$$J_\alpha := J_p+\frac{1}{4}m_pL_p^2.$$

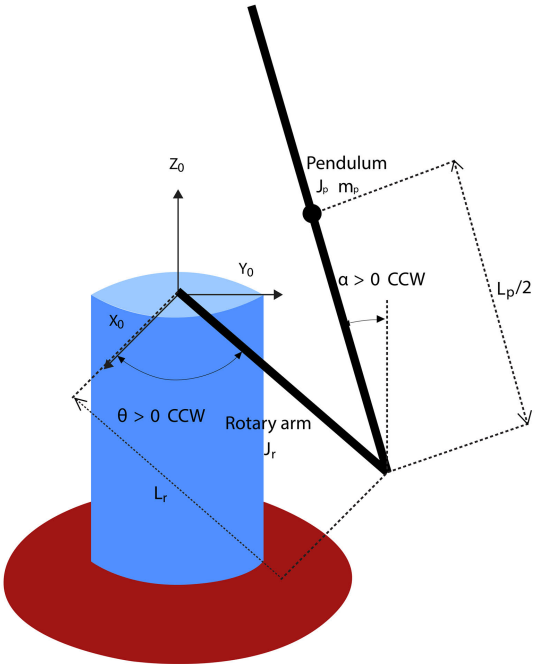

FIGURE 2. The rotary inverted pendulum conventions [24].

Note that, as shown from (1) and (2), the RotIPS belongs to a class of under-actuated mechanical system since there are two controlled outputs θ and α, but it has only one control input τ. We use the pendulum model in (2) to design the control algorithm in Section III.

Remark 1: We can observe that $J_\theta(\alpha) > 0, \forall\alpha \in [-\pi, \pi]$, which implies that the system dynamics described in (2) are always well-defined.

B. CONTROL OBJECTIVE

In this paper, the control objective is to drive the rotary arm (fully-actuated variable) from its initial position, $\theta(0)$, to reach the zero position and simultaneously stabilize the pendulum (under-actuated variable) in the vertical upright position from its initial position, $\alpha(0)$, based on the FBSTSA, which can be mathematically described as

$$\theta(t) \to 0,\ \alpha(t) \to 0.$$

Remark 2: The control problem considered in this paper is much more complicated than it may seem. The RotIPS belongs to a class of nonlinear, unstable, and under-actuated mechanical dynamic system. Hence, in order to apply the SMC approach, it requires a thorough mathematical examination. In contrast to the existing SMC approaches in [12]–[15], [22], [23], in this paper, we consider the second-order SMC stabilization control problem for the under-actuated RotIPS, which increases the complexity with respect to the control law design and stability analysis. We should mention that the problem of stabilization control for general under-actuated nonlinear systems is very challenging, and not limited to the under-actuated RotIPS. Further, we note that the proposed controller can be applied to other nonlinear under-

actuated systems including crane systems, ball and beam systems, and quadrotor and hexarotor UAV systems.

III. MAIN RESULTS

In this section, we propose a fuzzy-based super-twisting stabilization algorithm (FBSTSA) for the under-actuated RotIPS. We first introduce a new sliding surface to overcome the under-actuated structure. Then, together with the proposed sliding surface, we develop the FBSTSA, where the corresponding control gains are adjusted based on a fuzzy logic scheme.

We show that the proposed FBSTSA is capable of assuring the finite-time convergence to zero of the sliding variable during the reaching phase. Furthermore, the closed-loop system state converges to zero asymptotically during the sliding phase. We note that the proposed FBSTSA is continuous, whereas the existing SMC-based stabilization controllers for the under-actuated RotIPS are discontinuous [12]–[15].

We first design the FBSTSA for stabilization purpose. Then, we provide a rigorous stability analysis of the closed-loop system with the proposed control law.

A. FUZZY-BASED SUPER-TWISTING SLIDING MODE STABILIZATION CONTROL

1) CONTROL LAW DESIGN

In this subsection, the fuzzy-based super-twisting stabilization control scheme for the under-actuated RotIPS is presented. First, for the stabilization control objective, the sliding function s, which consists of the arm and the pendulum dynamics, is designed as follows:

$$s = k_\theta \dot{\theta} + k_\alpha \dot{\alpha} + \lambda_\theta \theta + \lambda_\alpha \alpha, \tag{3}$$

where k_θ, k_α, λ_θ, and λ_α are the sliding surface gains. Then, the super-twisting algorithm with the fuzzy variable gains is proposed as follows:

$$\begin{aligned}\tau &= -\frac{1}{k_\theta g_\theta(\alpha) + k_\alpha g_\alpha(\alpha)}\Big[k_\theta f_\theta\big(\alpha, \dot{\alpha}, \dot{\theta}\big) \\ &\quad + k_\alpha f_\alpha\big(\alpha, \dot{\alpha}, \dot{\theta}\big) + \lambda_\theta \dot{\theta} + \lambda_\alpha \dot{\alpha} + k_1(t)\phi_1(s) - z\Big] \\ \dot{z} &= -k_2(t)\phi_2(s),\end{aligned} \tag{4}$$

where ϕ_1 and ϕ_2 are given by

$$\begin{aligned}\phi_1(s) &= |s|^{1/2}\text{sign}(s) + k_3 s,\ k_3 > 0 \\ \phi_2(s) &= \frac{1}{2}\text{sign}(s) + \frac{3}{2}k_3|s|^{1/2}\text{sign}(s) + k_3^2 s.\end{aligned}$$

In the above expression, the gains k_1 and k_2 have the following form:

$$\begin{aligned}k_1(t) &= \frac{1}{2\beta_0}\Big[4\alpha_0(\beta_0 + 4\alpha_0^2) + 2\alpha_0 + K(t)\Big] \\ k_2(t) &= \beta_0 + 4\alpha_0^2 + 2\alpha_0 k_1(t),\end{aligned} \tag{5}$$

where α_0 and β_0 are positive scalar constants and K is determined via the fuzzy tuning mechanism presented in Section III-A2. Note that k_θ and k_α must be selected properly to ensure that $k_\theta g_\theta(\alpha) + k_\alpha g_\alpha(\alpha) \neq 0$ during the stabilization phase (see Remark 3).

2) FUZZY TUNING ALGORITHM DESIGN

For the fuzzy logic tuning mechanism, K is adjusted with regard to the absolute value of the sliding variable $|s|$ defined in (3). For simulation and experimental verification, the universes of discourse for $|s|$ and K are arranged as $[0, 1]$ and $[1, 40]$, respectively. The fuzzy input $|s|$ is defined as follows:

$$\{ZE,\ VT,\ T,\ AVG,\ B,\ VB,\ VVB\},$$

where ZE = Zero, VT = Very Tiny, T = Tiny, AVG = Average, B = Big, VB = Very Big, and VVB = Very Very Big, and the fuzzy output K is characterized by

$$\{VVT,\ VT,\ T,\ AVG,\ B,\ VB,\ VVB\},$$

where VVT = Very Very Tiny, VT = Very Tiny, T = Tiny, AVG = Average, B = Big, VB = Very Big, and VVB = Very Very Big. We use the triangle membership functions for both fuzzy input and output variables, as shown in Fig. 3.

From empirical knowledge of the design of the super-twisting algorithm, large switching gains will drive the state to the sliding surface s rapidly, but at the same time, they tend to enlarge the chattering phenomenon [22], [25], [26]. Hence, when the state is far from the sliding surface, the switching gains should be large, and they should be small when the state is close to the sliding surface.

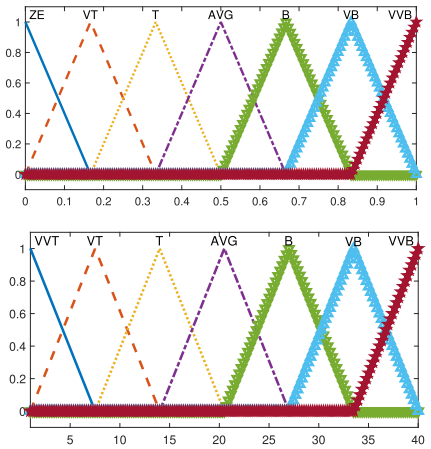

FIGURE 3. Membership functions: $|s|$ (top) and K (bottom).

According to the above analysis, the fuzzy rules are designed as shown in Table 3. The MIN-MAX methodology is used for the inference system. In addition, the defuzzification methodology used in the fuzzy logic scheme is of the centroid type. A detailed discussion of the membership function, inference system, and defuzzification methodology in fuzzy control can be found in [27]. In this paper, the fuzzy logic controller is designed using the fuzzy logic toolbox in MATLAB [28].

Before concluding this subsection, we provide several remarkable aspects of the implementation of the fuzzy mechanism in the super-twisting algorithm:

(i) the proposed FBSTSA reduces the chattering phenomenon, compared with the existing SMC approaches;

TABLE 3. Fuzzy rules for control gain K adjusting.

$\|s\|$	ZE	VT	T	AVG	B	VB	VVB
K	VVT	VT	T	AVG	B	VB	VVB

(ii) the proposed FBSTSA guarantees a faster reachability to the sliding surface than that with the existing SMC approaches; and
(iii) the proposed FBSTSA possesses better control accuracy owing to the adaptation of the switching gains with respect to the sliding variable, compared with the existing SMC approaches.

The features (i)–(iii) are verified through simulations and experiments in Sections IV and V.

B. STABILITY ANALYSIS

This subsection provides a stability analysis of the RotIPS in (2), with the proposed control law (4) in both the reaching and the sliding phases. We first prove that the proposed FBSTSA is capable of assuring the finite-time convergence to zero of the sliding variable during the reaching phase. Then, we show that, during the sliding phase, the closed-loop system achieves asymptotic stability.

1) REACHING PHASE STABILITY

By taking the derivative of (3), we have

$$\dot{s} = k_\theta \ddot{\theta} + k_\alpha \ddot{\alpha} + \lambda_\theta \dot{\theta} + \lambda_\alpha \dot{\alpha}. \tag{6}$$

Substituting (2) and (4) into (6) yields

$$\begin{aligned} \dot{s} &= -k_1(t)\phi_1(s) + z \\ \dot{z} &= -k_2(t)\phi_2(s). \end{aligned} \tag{7}$$

We have the following result:

Theorem 1: The sliding variable s described in (3) converges to zero in finite time if the controller gains k_1 and k_2 are defined as in (5). The finite convergence time to the sliding surface is approximated as

$$T = \frac{2}{\vartheta_2} \ln\left(\frac{\vartheta_2}{\vartheta_1} V^{1/2}(s(0), z(0)) + 1\right), \tag{8}$$

where $V(s,z) = \zeta^\top \mathbf{P}\zeta$, $\zeta^\top = \left[|s|^{1/2}\text{sign}(s) + k_3 s \;\; z\right]$, and ϑ_1 and ϑ_2 are described in (12).

Proof:

To prove the finite-time convergence of the sliding variable s, we construct an appropriate Lyapunov function and show that its derivative is negative with the proper controller gains.

In view of [22], consider the following Lyapunov candidate function:

$$V(s,z) = \zeta^\top \mathbf{P}\zeta, \tag{9}$$

where

$$\begin{aligned} \zeta^\top &= \left[|s|^{1/2}\text{sign}(s) + k_3 s \;\; z\right] \\ \mathbf{P} &= \begin{bmatrix} p_1 & p_3 \\ p_3 & p_2 \end{bmatrix} = \begin{bmatrix} \beta_0 + 4\alpha_0^2 & -2\alpha_0 \\ -2\alpha_0 & 1 \end{bmatrix}. \end{aligned} \tag{10}$$

We define $\mathtt{S} := \{(s,z) \in \mathbb{R}^2 : s = 0\}$. It can be observed that $V(s,z)$ is positive definite, continuous everywhere, and differentiable everywhere except on $\mathtt{S}$.

For every point in $\mathbb{R}^2 \setminus \mathtt{S}$, it follows from $\phi_2(s) := \phi_1'(s)\phi_1(s)$ that

$$\begin{aligned} \dot{\zeta} &= \begin{bmatrix} \phi_1'(s)\{-k_1(t)\phi_1(s) + z\} \\ -k_2(t)\phi_2(s) \end{bmatrix} = \phi_1'(s) \begin{bmatrix} -k_1(t) & 1 \\ -k_2(t) & 0 \end{bmatrix} \zeta \\ &:= \phi_1'(s)\overline{\mathbf{K}}(t)\zeta. \end{aligned}$$

We can see that the derivative of the function $V(s,z)$ in (9) exists on the same set, which can be obtained as follows:

$$\begin{aligned} \dot{V}(s,z) &= \phi_1'(s)\zeta^\top \left[\overline{\mathbf{K}}(t)^\top \mathbf{P} + \mathbf{P}\overline{\mathbf{K}}(t)\right]\zeta \\ &:= -\phi_1'(s)\zeta^\top \mathbf{Q}(t)\zeta, \end{aligned}$$

where $\mathbf{Q} := \begin{bmatrix} q_1 & q_3 \\ q_3 & q_2 \end{bmatrix}$ and

$$\begin{aligned} q_1(t) &:= 2k_1(t)p_1 + 2k_2(t)p_3 \\ q_2(t) &:= -2p_3 \\ q_3(t) &:= k_1(t)p_3 + k_2(t)p_2 - p_1. \end{aligned}$$

Selecting $\mathbf{P}$ as in (10), we can show that

$$\begin{aligned} q_1(t) &= 2k_1(t)(\beta_0 + 4\alpha_0^2) - 4\alpha_0 k_2(t) \\ q_2(t) &= 4\alpha_0 \\ q_3(t) &= -2\alpha_0 k_1(t) + k_2(t) - (\beta_0 + 4\alpha_0^2). \end{aligned} \tag{11}$$

From (11) and selecting the gains as in (5), we have

$$\mathbf{Q}(t) - 2\alpha_0 \mathbb{I} = \begin{bmatrix} K(t) & 0 \\ 0 & 2\alpha_0 \end{bmatrix},$$

where $\mathbb{I} \in \mathbb{R}^{2\times 2}$ is the identity matrix. We can observe that the proposed fuzzy scheme in Section III-A2 ensures the positive-definiteness of K, which then guarantees the positive-definiteness of the matrix $\mathbf{Q} - 2\alpha_0\mathbb{I}$. This leads to

$$\begin{aligned} \dot{V}(s,z) &= -\phi_1'(s)\zeta^\top \mathbf{Q}(t)\zeta \le -2\alpha_0 \phi_1'(s)\zeta^\top \zeta \\ &= -2\alpha_0 \left(\frac{1}{2|s|^{1/2}} + k_3\right)\zeta^\top \zeta. \end{aligned}$$

Since $\lambda_{\min}\{\mathbf{P}\}\|\zeta\|_2^2 \le V(s,z) \le \lambda_{\max}\{\mathbf{P}\}\|\zeta\|_2^2$, where $\|\zeta\|_2^2 = \zeta_1^2 + \zeta_2^2 = |s| + 2k_3|s|^{3/2} + k_3^2 s^2 + z^2$, and

$$|\zeta_1| \le \|\zeta\|_2 \le \frac{V^{1/2}(s,z)}{\lambda_{\min}^{1/2}\{\mathbf{P}\}},$$

it can be concluded that

$$\dot{V}(s,z) \le -\vartheta_1 V^{1/2}(s,z) - \vartheta_2 V(s,z), \tag{12}$$

where

$$\vartheta_1 = \frac{\alpha_0 \lambda_{\min}^{1/2}\{\mathbf{P}\}}{\lambda_{\max}\{\mathbf{P}\}}, \quad \vartheta_2 = \frac{2\alpha_0 k_3}{\lambda_{\max}\{\mathbf{P}\}}.$$

Note that the trajectories of (7) cannot stay on set $\mathtt{S}$ defined above. This implies that V is monotonically decreasing and the origin is finite-time stable [22].

To characterize the specific finite-time given in (8), we note that the solution of the comparison equation

$$\dot{v} = -\vartheta_1 v^{1/2} - \vartheta_2 v, \quad v(0) = v_0 \geq 0$$

can be obtained as

$$v(t) = \exp(-\vartheta_2 t)\left[v_0^{1/2} + \frac{\vartheta_1}{\vartheta_2}\left(1 - \exp\left(\frac{\vartheta_2}{2}t\right)\right)\right]^2.$$

This, together with (12) and the comparison principle [29], implies that the state dynamics in (7) converge to zero in finite time and reach that value at most after the time given in (8). This completes the proof of the theorem. ■

2) SLIDING PHASE STABILITY

In Section III-B1, we show that the sliding function s converges to zero in finite time T, where T is given in (8). Hence, from (3), the following holds in finite time:

$$\dot{\theta} = -\frac{\lambda_\theta}{k_\theta}\theta - \frac{\lambda_\alpha}{k_\theta}\alpha - \frac{k_\alpha}{k_\theta}\dot{\alpha}. \tag{13}$$

Note that Eq. (13) is always well-defined, since we can select $k_\theta \neq 0$ (see Remark 3).

We have the following result:

Theorem 2: During the sliding phase, the system state variables of the rotary inverted pendulum in (1), θ, $\dot{\theta}$, α, and $\dot{\alpha}$ are locally asymptotically stable if the sliding surface gains are selected as follows:

$$\lambda_\theta, k_\theta < 0, \quad \lambda_\alpha, k_\alpha > 0$$
$$\frac{\lambda_\alpha}{k_\alpha} > \frac{\lambda_\theta}{k_\theta}, \quad 2k_\theta J_\alpha + k_\alpha m_p L_p L_r > 0.$$

Proof: During the sliding phase, by substituting (4) and (13) into (2), the closed-loop dynamics of system (2) can be represented by

$$\ddot{\alpha} = f_\alpha(\theta, \alpha, \dot{\alpha}) - \frac{g_\alpha(\alpha)}{k_\theta g_\theta(\alpha) + k_\alpha g_\alpha(\alpha)}\Big[k_\theta f_\theta(\theta, \alpha, \dot{\alpha}) + k_\alpha f_\alpha(\theta, \alpha, \dot{\alpha}) + \lambda_\theta\Big(-\frac{\lambda_\theta}{k_\theta}\theta - \frac{\lambda_\alpha}{k_\theta}\alpha - \frac{k_\alpha}{k_\theta}\dot{\alpha}\Big) + \lambda_\alpha\dot{\alpha}\Big]$$

$$k_\theta\ddot{\theta} + k_\alpha\ddot{\alpha} + \lambda_\theta\theta + \lambda_\alpha\alpha = 0. \tag{14}$$

Let $x_1 = \theta$, $x_2 = \alpha$, and $x_3 = \dot{\alpha}$ and $\mathbf{x} = \begin{bmatrix} x_1 & x_2 & x_3 \end{bmatrix}^\top$. From (14), we can form a new dynamical system as

$$\dot{\mathbf{x}} = \mathbf{f}(\mathbf{x}) = \begin{bmatrix} f_1(\mathbf{x}) \\ f_2(\mathbf{x}) \\ f_3(\mathbf{x}) \end{bmatrix}, \tag{15}$$

where

$$f_1(\mathbf{x}) := -\frac{\lambda_\theta}{k_\theta}x_1 - \frac{\lambda_\alpha}{k_\theta}x_2 - \frac{k_\alpha}{k_\theta}x_3$$
$$f_2(\mathbf{x}) := x_3$$
$$f_3(\mathbf{x}) := f_\alpha(x_1, x_2, x_3) - \frac{g_\alpha(x_2)}{k_\theta g_\theta(x_2) + k_\alpha g_\alpha(x_2)} \times \Big[k_\theta f_\theta(x_1, x_2, x_3) + k_\alpha f_\alpha(x_1, x_2, x_3) + \lambda_\theta\Big(-\frac{\lambda_\theta}{k_\theta}x_1 - \frac{\lambda_\alpha}{k_\theta}x_2 - \frac{k_\alpha}{k_\theta}x_3\Big) + \lambda_\alpha x_3\Big],$$

where the definition of $f_\theta(x_1, x_2, x_3)$, $f_\alpha(x_1, x_2, x_3)$, $g_\theta(x_2)$, and $g_\alpha(x_2)$ are given in (16), as shown at the bottom of the page.

The stability of the autonomous system given by (15) must be investigated. First, we can easily check that the equilibrium point of (15) is the origin, that is, $\mathbf{x}_e = \mathbf{0}$. Then by linearizing the system (15) around the equilibrium point, the following linearized system can be obtained:

$$\dot{\mathbf{x}} = \mathbf{A}\mathbf{x}, \tag{17}$$

where $\mathbf{A} = \frac{\partial \mathbf{f}(\mathbf{x})}{\partial \mathbf{x}}\Big|_{\mathbf{x}=\mathbf{x}_e} = \begin{bmatrix} A^{11} & A^{12} & A^{13} \\ A^{21} & A^{22} & A^{23} \\ A^{31} & A^{32} & A^{33} \end{bmatrix}$ with elements defined by

$$A^{11} := -\frac{\lambda_\theta}{k_\theta}, \; A^{12} := -\frac{\lambda_\alpha}{k_\theta}, \; A^{13} := -\frac{k_\alpha}{k_\theta}$$
$$A^{21} := 0, \; A^{22} := 0, \; A^{23} := 1$$
$$A^{31} := \frac{\lambda_\theta^2}{k_\theta}\frac{m_p L_p L_r}{2k_\theta J_\alpha + k_\alpha m_p L_p L_r}$$

$$f_\theta(x_1, x_2, x_3) := \frac{4J_\alpha}{J_\theta(x_2)}\Big[\Big(-\frac{\lambda_\theta}{k_\theta}x_1 - \frac{\lambda_\alpha}{k_\theta}x_2 - \frac{k_\alpha}{k_\theta}x_3\Big)\Big(-\frac{1}{2}m_p L_p^2 \sin(x_2)\cos(x_2)x_3\Big) + \Big(-\frac{\lambda_\theta}{k_\theta}x_1 - \frac{\lambda_\alpha}{k_\theta}x_2 - \frac{k_\alpha}{k_\theta}x_3\Big)^2\Big(\frac{1}{8J_\alpha}m_p^2 L_p^3 L_r \sin(x_2)\cos^2(x_2)\Big) - \frac{1}{2}m_p L_p L_r \sin(x_2)x_3^2 + \frac{1}{4J_\alpha}m_p^2 L_p^2 L_r g \sin(x_2)\cos(x_2)\Big]$$

$$f_\alpha(x_1, x_2, x_3) := \frac{1}{J_\theta(x_2)}m_p L_p L_r \cos(x_2)\Big[-m_p L_p^2 \sin(x_2)\cos(x_2)x_3\Big(-\frac{\lambda_\theta}{k_\theta}x_1 - \frac{\lambda_\alpha}{k_\theta}x_2 - \frac{k_\alpha}{k_\theta}x_3\Big) - m_p L_p L_r \sin(x_2)x_3^2\Big] + \frac{1}{4J_\theta(x_2)}m_p L_p^2 \sin(x_2)\cos(x_2)\Big(-\frac{\lambda_\theta}{k_\theta}x_1 - \frac{\lambda_\alpha}{k_\theta}x_2 - \frac{k_\alpha}{k_\theta}x_3\Big)^2\Big(4\bar{J}_r + m_p L_p^2 \sin^2(x_2)\Big) + \frac{1}{2J_\theta(x_2)}m_p L_p g \sin(x_2)\Big(4\bar{J}_r + m_p L_p^2 \sin^2(x_2)\Big)$$

$$g_\theta(x_2) := \frac{4J_\alpha}{J_\theta(x_2)}, \; g_\alpha(x_2) := \frac{2}{J_\theta(x_2)}m_p L_p L_r \cos(x_2), \; J_\theta(x_2) := 4J_\alpha\bar{J}_r + J_\alpha m_p L_p^2 \sin^2(x_2) - m_p^2 L_p^2 L_r^2 \cos^2(x_2). \tag{16}$$

$$A^{32} := \frac{1}{k_\theta}\frac{m_p L_p g k_\theta^2 + m_p L_p L_r \lambda_\theta \lambda_\alpha}{2k_\theta J_\alpha + k_\alpha m_p L_p L_r}$$
$$A^{33} := -\frac{m_p L_p L_r}{2k_\theta J_\alpha + k_\alpha m_p L_p L_r}\Big(-\frac{\lambda_\theta k_\alpha}{k_\theta} + \lambda_\alpha\Big).$$

We note that the origin of (17) is asymptotically stable if all eigenvalues of $\mathbf{A}$ are in the open left-half of the complex plane. Let us define $\overline{\mathbf{A}} := \rho\bar{\mathbb{I}} - \mathbf{A}$, where ρ is the Laplace variable and $\bar{\mathbb{I}} \in \mathbb{R}^{3\times 3}$ is the identity matrix. Then, $\overline{\mathbf{A}}$ can be expressed as follows:

$$\overline{\mathbf{A}} := \begin{bmatrix} \overline{A}^{11} & \overline{A}^{12} & \overline{A}^{13} \\ \overline{A}^{21} & \overline{A}^{22} & \overline{A}^{23} \\ \overline{A}^{31} & \overline{A}^{32} & \overline{A}^{33} \end{bmatrix}$$

where

$$\overline{A}^{11} := \rho + \frac{\lambda_\theta}{k_\theta},\ \overline{A}^{12} := \frac{\lambda_\alpha}{k_\theta},\ \overline{A}^{13} := \frac{k_\alpha}{k_\theta}$$
$$\overline{A}^{21} := 0,\ \overline{A}^{22} := \rho,\ \overline{A}^{23} := -1$$
$$\overline{A}^{31} := -\frac{\lambda_\theta^2}{k_\theta}\frac{m_p L_p L_r}{2k_\theta J_\alpha + k_\alpha m_p L_p L_r}$$
$$\overline{A}^{32} := -\frac{1}{k_\theta}\frac{m_p L_p g k_\theta^2 + m_p L_p L_r \lambda_\theta \lambda_\alpha}{2k_\theta J_\alpha + k_\alpha m_p L_p L_r}$$
$$\overline{A}^{33} := \rho + \frac{m_p L_p L_r}{2k_\theta J_\alpha + k_\alpha m_p L_p L_r}\Big(-\frac{\lambda_\theta k_\alpha}{k_\theta} + \lambda_\alpha\Big).$$

Hence, we obtain the characteristic equation of system (17), which can be written as

$$\rho^3 + \rho^2\Big[\frac{\lambda_\theta}{k_\theta} + \frac{m_p L_p L_r}{2k_\theta J_\alpha + k_\alpha m_p L_p L_r}\Big(-\frac{\lambda_\theta k_\alpha}{k_\theta} + \lambda_\alpha\Big)\Big] + \rho\Big[-\frac{m_p L_p g k_\theta}{2k_\theta J_\alpha + k_\alpha m_p L_p L_r}\Big] + \Big[-\frac{m_p L_p g \lambda_\theta}{2k_\theta J_\alpha + k_\alpha m_p L_p L_r}\Big] = 0. \quad (18)$$

Note that the equilibrium point of (17) is asymptotically stable when the roots of the polynomial in (18) are in the open left-half plane of the complex domain. This can be achieved if the sliding surface gains $k_\theta, k_\alpha, \lambda_\theta$, and λ_α are chosen to satisfy the following conditions:

$$\lambda_\theta, k_\theta < 0, \quad \lambda_\alpha, k_\alpha > 0 \quad (19)$$
$$\frac{\lambda_\alpha}{k_\alpha} > \frac{\lambda_\theta}{k_\theta}, \quad 2k_\theta J_\alpha + k_\alpha m_p L_p L_r > 0.$$

It should be pointed out that it is always possible to select the sliding surface gains $k_\theta, k_\alpha, \lambda_\theta$, and λ_α such that (19) is satisfied (see Remark 3). The conditions given in (19) ensure that all eigenvalues of $\mathbf{A}$ are in the open left-half of the complex plane. Hence, θ, α, and $\dot{\alpha}$ are asymptotically stable. Then, Eq. (13) assures that $\dot{\theta}$ is asymptotically stable. In other words, if $k_\theta, k_\alpha, \lambda_\theta$, and λ_α are selected to satisfy (19), then the linear system given in (17) is asymptotically stable, which leads to the stability of the nonlinear system given by (15) around the equilibrium point [29]. This completes the proof of the theorem. ■

Before concluding this section, we provide several important remarks on the proposed FBSTSA.

Remark 3:

(i) For the effective implementation of the proposed controller, the sliding surface gains need to be selected carefully. The following tuning procedure can be applied to determine the proper parameters:
   1) Without loss of generality, set
   $$k_\theta = -0.1, \lambda_\theta = -0.1$$
   to satisfy the condition $\lambda_\theta, k_\theta < 0$.
   2) With $k_\theta = -0.1$, k_α is taken as 0.2 to satisfy the following conditions
   $$2k_\theta J_\alpha + k_\alpha m_p L_p L_r > 0,\ k_\alpha > 0.$$
   3) Maintain $k_\theta = -0.1, \lambda_\theta = -0.1$, and $k_\alpha = 0.2$, tune λ_α by increasing from a small value, while checking the errors and vibrations, as well as the conditions $\frac{\lambda_\alpha}{k_\alpha} > \frac{\lambda_\theta}{k_\theta}$ and $\lambda_\alpha > 0$.

(ii) With $k_\theta = -0.1, \lambda_\theta = -0.1, k_\alpha = 0.2$, and $\lambda_\alpha = 3.1$, we have the following results:
   - The conditions given in (19) are satisfied.
   - By selecting $k_\theta = -0.1,\ k_\alpha = 0.2$, we can verify that $k_\theta g_\theta(\alpha) + k_\alpha g_\alpha(\alpha) \neq 0,\ \forall\alpha \in [-1, 1]$ (rad). In this work, we start the stabilization procedure when $\alpha \in [-\frac{\pi}{15}, \frac{\pi}{15}]$ (rad), which implies that the proposed stabilization control law in (4) is always well-defined.

(iii) The structure of the proposed FBSTSA (4) is simple. We can implement this controller easily in practice. We also note that, as mentioned in Section III-A2, the fuzzy logic controller can be easily implemented using available fuzzy logic toolboxes such as the MATLAB software [28].

The following remark presents the main contributions of our paper and provides a comparison with the existing approaches (see also Introduction):

Remark 4:

(i) Although different SMC approaches have been employed successfully for various fully-actuated systems, it is difficult to apply these methods directly for under-actuated systems, in particular, for the stabilization control of the under-actuated RotIPS in (2). The main obstacle is how to define a sliding surface that can simultaneously stabilize both fully-actuated (rotary arm) and under-actuated (pendulum) variables, especially when the system (1) shows high-nonlinearities and complex couplings. To address this problem, we proposed the new sliding surface in (3), which ensures the asymptotic stability of both the fully-actuated and the under-actuated variables.

(ii) Note that the stability proof for Theorems 1 and 2 is different from that of [12]–[15], [22], [23]. In particular, in our proof, we show that: (i) by defining proper fuzzy variable gains, the proposed FBSTSA can force

the sliding variable to zero in finite time using the *continuous* control law (see Theorem 1); and (ii) after the system state converges to the designed sliding surface (3), the asymptotic stability of the closed-loop system can be achieved in the sliding phase by selecting proper sliding surface gains (see Theorem 2). Hence, Theorem 1 together with Theorem 2 overcome the two main drawbacks mentioned in Introduction when applying the SMC for the under-actuated RotIPS.

(iii) Finally, it should be noted that the existing super-twisting algorithms in [22], [23] cannot be used directly for the stabilization control of the under-actuated RotIPS because of two reasons: (i) their sliding surfaces were proposed only for fully-actuated systems; and (ii) as shown in Theorem 2, the sliding variable is required to reach zero in finite time in order to ensure the asymptotic stability of the closed-loop system, whereas the adaptive gains in [23] only ensure the finite-time convergence of the sliding variable to a small region around zero.

The following remark discusses some potential research topics for our future works:

Remark 5: In this paper, we have not considered the influence of the input saturation on the system actuator during the control design. Hence, the control parameters must be chosen carefully to avoid violating the actuator constraints of the experimental hardware system. This problem will be addressed in our future work. The readers are referred to [30], [31] for effective methods to solve the actuator constraint problems. In addition, it would be interesting to develop an output-feedback stabilization controller for the RotIPS based on the proposed FBSTSA together with the velocity estimation approach, as reported in [32], [33]. Another possible future research direction is to consider the stabilization control design for the RotIPS under additive matched and mismatched disturbances. Finally, we can also apply the proposed FBSTSA to the power system load frequency control problem [34], [35].

IV. SIMULATION RESULTS

In this section, we provide the simulation setup, simulation procedure, and detailed analysis and discussion of the simulation results.

A. SIMULATION SETUP

We consider various simulation control scenarios to illustrate the effectiveness of the proposed FBSTSA for the under-actuated RotIPS. We illustrate that the proposed FBSTSA can simultaneously stabilize the arm and the pendulum.

The parameters of the Quanser rotary inverted pendulum are selected as in [24]. The simulation is performed by starting to stabilize the system from the initial conditions of $\alpha(0) = -\frac{\pi}{15}$ (rad), $\theta(0) = 0$ (rad), $\dot{\alpha}(0) = \dot{\theta}(0) = 0$ (rad/s).

To validate the performance of the proposed FBSTSA, we investigate the following two simulation groups:

Group 1: (*Comparison performance*) We demonstrate the superior stabilization control performance of the proposed FBSTSA by comparing it with the decoupled SMC (DSMC) [12] and the SMC [13];

Group 2: (*Robustness verification*) We verify the robustness of the proposed FBSTSA in the following two control cases:

– Case 1: (*System uncertainties*) We illustrate the robustness of the proposed FBSTSA with respect to system uncertainties. The system parameters including uncertainties are modeled as follows:

$$m_p := m_p + \Delta m_p,\ L_p := L_p + \Delta L_p,$$

where Δm_p and ΔL_p represent the modeling uncertainties with $\pm 20\%$ discrepancy from the nominal values. The FBSTSA is designed using nominal parameters.

– Case 2: (*External disturbances*) We examine the control performance of the proposed FBSTSA under the effect of sudden external disturbances. At 10 (sec) and 20 (sec), control torques of 0.5 (N.m) and -0.5 (N.m) are added to the control effort during 0.05 (sec), respectively.

B. SIMULATION EVALUATION

In this subsection, the corresponding results of the two simulation groups are presented.

1) GROUP 1

In this Group, the proposed FBSTSA is compared with the other two SMC-based controllers for stabilizing the RotIPS, including the DSMC in [12] and the SMC in [13]. For the sake of fair comparisons (e.g., control accuracy, chattering alleviation, and convergence rate), the control input torque is bounded by 2 (N.m). The simulation results of stabilization control for the RotIPS by all three controllers are depicted in Fig. 4.

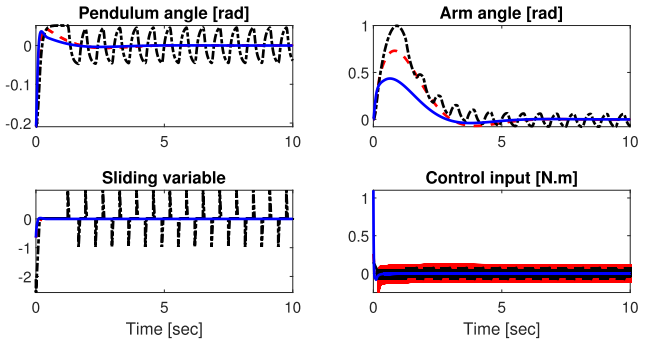

FIGURE 4. Simulation results – Group 1. DSMC [12] (dash-dot black), SMC [13] (dashed red), and proposed FBSTSA (solid blue).

2) GROUP 2

For Group 2, we illustrate the robustness of the proposed FBSTSA in the following two control scenarios:

CASE 1

We consider the ability of the proposed FBSTSA to attenuate the effect of parametric variations by adding modeling uncertainties into the nominal dynamic model. Note that the proposed FBSTSA still uses nominal system parameters. The simulation results with the effect of the system uncertainties are shown in Figs. 5 and 6.

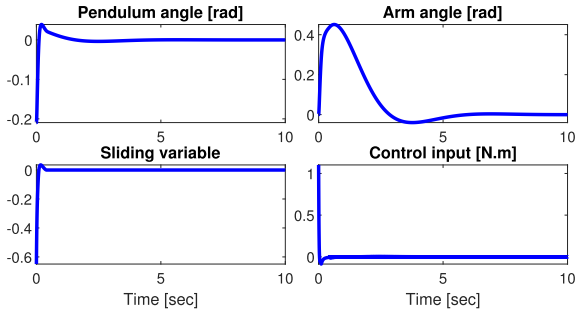

FIGURE 5. Simulation results – Group 2 (Case 1 – 20% increased).

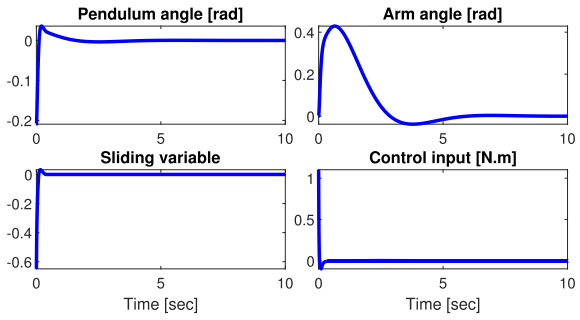

FIGURE 6. Simulation results – Group 2 (Case 1 – 20% decreased).

CASE 2

The proposed FBSTSA's immunity against bounded sudden external disturbances is investigated by injecting two pulse torque signals in the control input torque. The magnitudes of these signals are 0.5 (N.m) and −0.5 (N.m), and their durations are 0.05 (sec) at 10 (sec) and 20 (sec), respectively. Fig. 7 depicts the performance of the proposed FBSTSA against the sudden external disturbances.

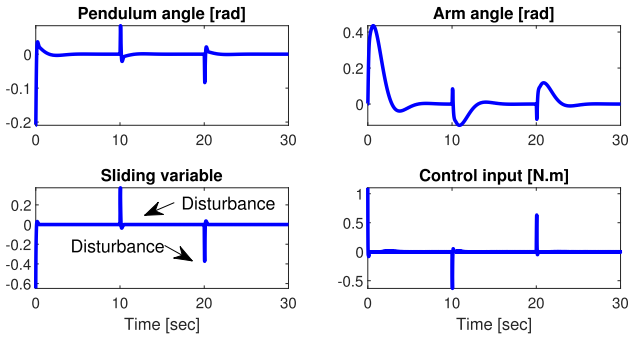

FIGURE 7. Simulation results – Group 2 (Case 2).

C. ANALYSIS AND DISCUSSION

In Group 1, as shown in Fig. 4, we can observe that the proposed FBSTSA provides better control accuracy, compared with the DSMC [12] and the SMC [13]. In this paper, we also use the root-mean-square error (RMSE) and convergence time (CT) as performance indexes in order to evaluate the control performance of the DSMC, the SMC, and the proposed FBSTSA. CT is the time after which $|\alpha| \leq \frac{\pi}{60}$ (rad) and $|\theta| \leq \frac{\pi}{15}$ (rad) are satisfied. As seen from Table 4, the proposed FBSTSA shows the minimum RMSE, as well as the fastest CT. With regard to the chattering alleviation ability, we can observe from Fig. 4 that the DSMC and the SMC show serious chattering in the control torque, while the proposed FBSTSA attenuates the chattering effectively. Hence, the simulation results in Group 1 show that chattering phenomenon is alleviated and better control performance is achieved by the proposed FBSTSA, compared with the existing SMCs in [12], [13].

TABLE 4. Simulation performance comparison – Group 1.

	DSMC [12]	SMC [13]	Proposed FBSTSA
RMSE of the arm angle (rad)	0.329	0.264	0.155
RMSE of the pendulum angle (rad)	0.040	0.021	0.014
CT (sec)	2.658	2.278	1.758

For Group 2, with the influence of system uncertainties and external disturbances shown in Figs. 5, 6, and 7, robust performance is achieved with the proposed FBSTSA. It can be seen that the proposed controller responds rapidly to drive the arm to the zero position and stabilize the pendulum in its upright position at the same time.

In summary, from the simulation results of Groups 1 and 2, we can conclude that the proposed FBSTSA safeguards the stability and robustness of the closed-loop systems under different operating conditions.

V. EXPERIMENTAL RESULTS

This section first describes the hardware experiment configuration, then presents the experimental examination, and finally, provides detailed analysis and discussion with regard to the experimental results.

A. EXPERIMENT SETUP

Extensive experimental validation is conducted on the rotary inverted pendulum built by the Quanser company, as shown in Fig. 8. The hardware includes the following components: (i) the rotary inverted pendulum, which is equipped with a DC motor and two encoders to read the rotary arm and the pendulum angles; (ii) the built-in PWM power amplifier device; and (iii) the data acquisition device. These hardware components are connected to a laptop through the USB interface provided by Quanser. To drive the DC motor and read the arm and the pendulum angles, we use the QUARC real-time control software, integrated with MATLAB/Simulink [24]. The output voltage range of the load is between ±5V. The block diagram for the real-time implementation is illustrated in Fig. 9.

It should be noted that the energy-based control method [36] is used to drive the pendulum to a close region around an unstable equilibrium point. Then, the stabilization procedure is triggered when $\alpha \in [-\frac{\pi}{15}, \frac{\pi}{15}]$ (rad).

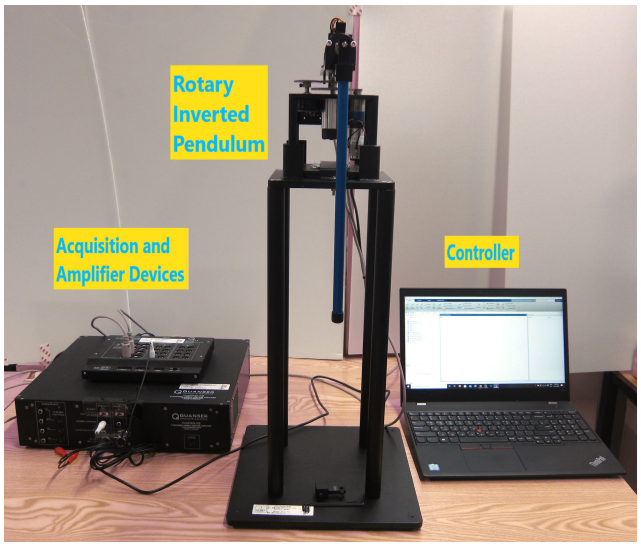

FIGURE 8. Experiment configuration.

For experimental verification, we conduct the following two different experiments:

Group 1: (*Comparison performance*) The superiority of the proposed FBSTSA is illustrated by comparing it with the DSMC [12] and the SMC [13];

Group 2: (*Robustness verification*) We verify the robustness of the proposed FBSTSA in the following two cases:

– Case 1: (*Different initial conditions*) We consider the robustness of the proposed FBSTSA with respect to different initial conditions. In order to generate different initial conditions compared with Group 1, we trigger the stabilization procedure when $\alpha \in [-\frac{\pi}{9}, \frac{\pi}{9}]$ (rad). Note also that we use different control parameters for the energy-based swing-up controller [36].

– Case 2: (*External disturbances*) We evaluate the control performance of the proposed FBSTSA under the effect of external disturbances. To produce the sudden external disturbances, we interrupt the motion of the pendulum by a push-pull perturbation.

We mention that all the experiment results as a movie clip are available at https://drive.google.com/file/d/1xAr30XJxpkAKWvuj0LyQjYAd1Kwy-g9j/view.

B. EXPERIMENT EVALUATION

In this subsection, we present the corresponding experimental results of two experiment groups.

1) GROUP 1

In this Group, we compare the stabilization control performance of the proposed FBSTSA with the DSMC [12] and the SMC [13]. Fig. 10 depicts the corresponding experimental results of the DSMC, the SMC, and the proposed FBSTSA, respectively.

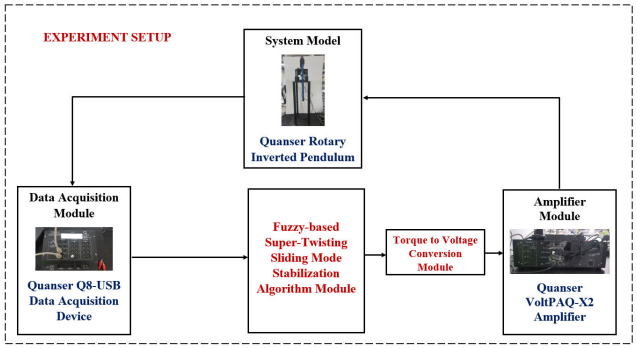

FIGURE 9. Block diagram for the real-time implementation.

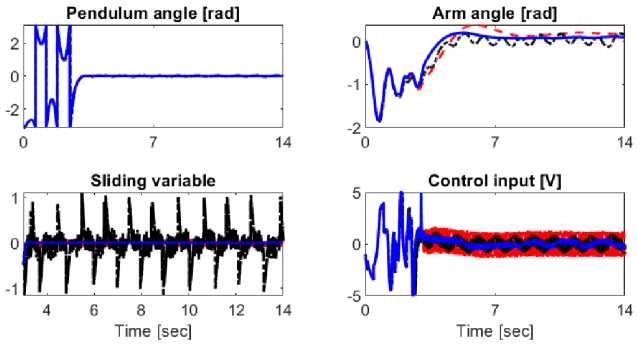

FIGURE 10. Experimental results – Group 1. DSMC [12] (dash-dot black), SMC [13] (dashed red), and proposed FBSTSA (solid blue).

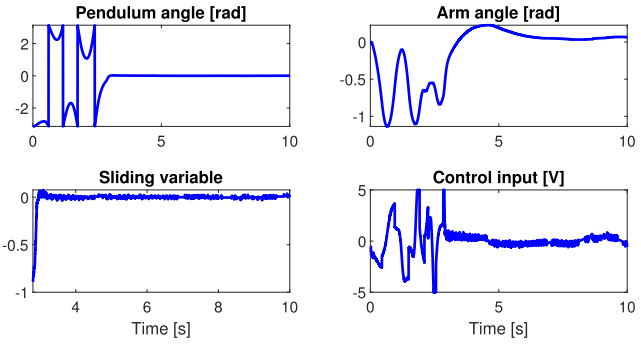

FIGURE 11. Experimental results – Group 2 (Case 1).

2) GROUP 2

For Group 2, we verify the robustness of the proposed FBSTSA in the following two control cases:

CASE 1

The proposed FBSTSA's ability to resist system parameter uncertainties is considered. The stabilization procedure is triggered when $\alpha \in [-\frac{\pi}{9}, \frac{\pi}{9}]$ (rad). In addition, we change the control parameters of the energy-based swing-up controller in [36] to generate different initial conditions compared with the initial system states in experiment Group 1. The experimental results with regard to the system uncertainties are depicted in Fig. 11.

CASE 2

In this control scenario, we investigate the robustness of the proposed FBSTSA in the presence of sudden exter-

nal disturbances. As marked in Fig. 12, the external disturbance appears two times at approximately 28 (sec) and at approximately 46 (sec), respectively. The corresponding experimental results of the closed-loop system are shown in Fig. 12.

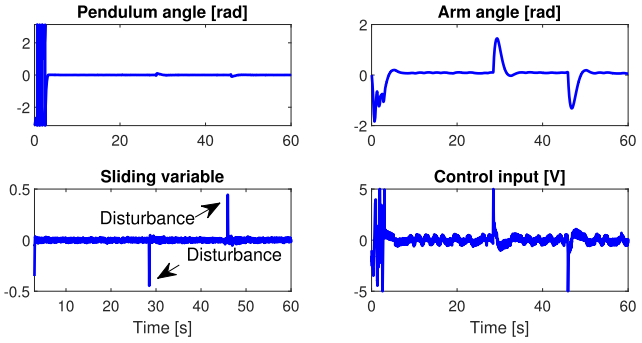

FIGURE 12. Experimental results – Group 2 (Case 2).

C. ANALYSIS AND DISCUSSION

In Group 1, as shown in Fig. 10, we can observe that the proposed FBSTSA provides the chattering reduction ability, a faster convergence rate, and improved control accuracy, compared with the DSMC [12] and the SMC [13]. More quantitatively, the RMSE is computed for each control algorithm to show the advantages of the proposed FBSTSA. Table 5 shows the RMSE of the arm and the pendulum angles for all three control methods. In addition, in Table 5, we compare the CT of three control methods. CT is the time after which $|\alpha| \leq \frac{\pi}{60}$ (rad) and $|\theta| \leq \frac{\pi}{15}$ (rad) are satisfied. As seen from Table 5, the proposed FBSTSA attains the minimum RMSE and shows the faster CT, compared with [12], [13]. The experimental results presented in Group 1 show that chattering phenomenon is alleviated and better control performance is achieved by the proposed FBSTSA, compared with the existing SMC approaches in [12], [13].

TABLE 5. Experimental performance comparison – Group 1.

	DSMC [12]	SMC [13]	Proposed FBSTSA
RMSE of the arm angle (rad)	0.195	0.296	0.151
RMSE of the pendulum angle (rad)	0.036	0.017	0.013
CT (sec)	13.166	7.428	3.622

For Group 2, we verify the robustness of the proposed FBSTSA against system parameter uncertainties and external disturbances. From Figs. 11 and 12, we can observe that the proposed FBSTSA responds rapidly to stabilize the pendulum and arm around its zero position in the presence of parameter uncertainties and external disturbances.

In summary, from the presented experimental results, we can conclude that the proposed FBSTSA can guarantee stability and robustness of the closed-loop system under various control situations.

VI. CONCLUSION AND FUTURE WORKS

In this paper, the stabilization problem of the unstable under-actuated rotary pendulum system (RotIPS) was considered via the fuzzy-based (continuous) super-twisting stabilization algorithm (FBSTSA). To address the under-actuated dynamic, a new sliding surface was defined. To reduce the chattering and enhance the control performance, the control gains of the proposed FBSTSA were adjusted based on a fuzzy logic scheme depending on the value of the sliding variable. We have shown that, with the proposed FBSTSA, the sliding variable is driven to zero in finite time and the closed-loop system converges to zero asymptotically. Various simulation and experimental results for the under-actuated RotIPS were provided to validate the performance of the proposed FBSTSA.

One possible future research direction is to develop the stabilization controller for the RotIPS with actuator constraints. In addition, it would be interesting to develop an output-feedback stabilization control law for the RotIPS by integrating the proposed FBSTSA with the velocity estimator/observer. Another possible future research direction is to consider the stabilization control design for the RotIPS under additive matched and mismatched disturbances. Finally, we can also apply the proposed FBSTSA to the load frequency control problem in power systems.

REFERENCES

[1] O. Boubaker, "The inverted pendulum benchmark in nonlinear control theory: A survey," *Int. J. Adv. Robotic Syst.*, vol. 10, no. 5, p. 233, May 2013.
[2] M. F. Hamza, H. J. Yap, I. A. Choudhury, A. I. Isa, A. Y. Zimit, and T. Kumbasar, "Current development on using rotary inverted pendulum as a benchmark for testing linear and nonlinear control algorithms," *Mech. Syst. Signal Process.*, vol. 116, pp. 347–369, Feb. 2019.
[3] V. M. Hernández-Guzmán, M. Antonio-Cruz, and R. Silva-Ortigoza, "Linear state feedback regulation of a furuta pendulum: Design based on differential flatness and root locus," *IEEE Access*, vol. 4, pp. 8721–8736, 2016.
[4] P. Dwivedi, S. Pandey, and A. S. Junghare, "Stabilization of unstable equilibrium point of rotary inverted pendulum using fractional controller," *J. Franklin Inst.*, vol. 354, no. 17, pp. 7732–7766, Nov. 2017.
[5] X. Yang and X. Zheng, "Swing-up and stabilization control design for an underactuated rotary inverted pendulum system: Theory and experiments," *IEEE Trans. Ind. Electron.*, vol. 65, no. 9, pp. 7229–7238, Sep. 2018.
[6] T. Horibe and N. Sakamoto, "Optimal swing up and stabilization control for inverted pendulum via stable manifold method," *IEEE Trans. Control Syst. Technol.*, vol. 26, no. 2, pp. 708–715, Mar. 2018.
[7] H. Gritli and S. Belghith, "Robust feedback control of the underactuated inertia wheel inverted pendulum under parametric uncertainties and subject to external disturbances: LMI formulation," *J. Franklin Inst.*, vol. 355, no. 18, pp. 9150–9191, Dec. 2018.
[8] Y.-F. Chen and A.-C. Huang, "Adaptive control of rotary inverted pendulum system with time-varying uncertainties," *Nonlinear Dyn.*, vol. 76, no. 1, pp. 95–102, Apr. 2014.
[9] R. Cui, J. Guo, and Z. Mao, "Adaptive backstepping control of wheeled inverted pendulums models," *Nonlinear Dyn.*, vol. 79, no. 1, pp. 501–511, Jan. 2015.
[10] J. Huang, M. Ri, D. Wu, and S. Ri, "Interval type-2 fuzzy logic modeling and control of a mobile two-wheeled inverted pendulum," *IEEE Trans. Fuzzy Syst.*, vol. 26, no. 4, pp. 2030–2038, Aug. 2018.
[11] X. Su, F. Xia, J. Liu, and L. Wu, "Event-triggered fuzzy control of nonlinear systems with its application to inverted pendulum systems," *Automatica*, vol. 94, pp. 236–248, Aug. 2018.
[12] R. Coban and B. Ata, "Decoupled sliding mode control of an inverted pendulum on a cart: An experimental study," in *Proc. IEEE Int. Conf. Adv. Intell. Mechatronics (AIM)*, Jul. 2017, pp. 993–997.

[13] A. Wadi, J.-H. Lee, and L. Romdhane, "Nonlinear sliding mode control of the furuta pendulum," in *Proc. 11th Int. Symp. Mechatronics Appl. (ISMA)*, Mar. 2018, pp. 1–5.
[14] B. A. Elsayed, M. A. Hassan, and S. Mekhilef, "Fuzzy swinging-up with sliding mode control for third order cart-inverted pendulum system," *Int. J. Control, Autom. Syst.*, vol. 13, no. 1, pp. 238–248, Feb. 2015.
[15] I. M. Mehedi, U. Ansari, A. H. Bajodah, U. M. Al-Saggaf, B. Kada, and M. J. Rawa, "Underactuated rotary inverted pendulum control using robust generalized dynamic inversion," *J. Vib. Control*, early access, Mar. 20, 2020, doi: 10.1177/1077546320916022.
[16] V. Utkin, J. Guldner, and J. Shi, *Sliding Mode Control in Electro-Mechanical Systems*. Boca Raton, FL, USA: CRC Press, 2009.
[17] A. Levant, "Sliding order and sliding accuracy in sliding mode control," *Int. J. Control*, vol. 58, no. 6, pp. 1247–1263, Dec. 1993.
[18] V. I. Utkin, "Sliding mode control design principles and applications to electric drives," *IEEE Trans. Ind. Electron.*, vol. 40, no. 1, pp. 23–36, Feb. 1993.
[19] J. Hu, Y. Cui, C. Lv, D. Chen, and H. Zhang, "Robust adaptive sliding mode control for discrete singular systems with randomly occurring mixed time-delays under uncertain occurrence probabilities," *Int. J. Syst. Sci.*, vol. 51, no. 6, pp. 987–1006, Apr. 2020.
[20] Y. Wang, B. Jiang, Z.-G. Wu, S. Xie, and Y. Peng, "Adaptive sliding mode fault-tolerant fuzzy tracking control with application to unmanned marine vehicles," *IEEE Trans. Syst., Man, Cybern., Syst.*, pp. 1–10, 2020.
[21] Y. Wang, X. Xie, M. Chadli, S. Xie, and Y. Peng, "Sliding mode control of fuzzy singularly perturbed descriptor systems," *IEEE Trans. Fuzzy Syst.*, early access, May 29, 2020, doi: 10.1109/TFUZZ.2020.2998519.
[22] J. A. Moreno and M. Osorio, "Strict Lyapunov functions for the super-twisting algorithm," *IEEE Trans. Autom. Control*, vol. 57, no. 4, pp. 1035–1040, Apr. 2012.
[23] Y. Shtessel, M. Taleb, and F. Plestan, "A novel adaptive-gain supertwisting sliding mode controller: Methodology and application," *Automatica*, vol. 48, no. 5, pp. 759–769, May 2012.
[24] *Instructor Workbook—Inverted Pendulum Experiment for MATLAB/Simulink Users*, Markham, ON, Canada, 2011.
[25] A. Vargas, J. A. Moreno, and A. Vande Wouwer, "A weighted variable gain super-twisting observer for the estimation of kinetic rates in biological systems," *J. Process Control*, vol. 24, no. 6, pp. 957–965, Jun. 2014.
[26] R. Seeber and M. Horn, "Stability proof for a well-established super-twisting parameter setting," *Automatica*, vol. 84, pp. 241–243, Oct. 2017.
[27] K. M. Passino, S. Yurkovich, and M. Reinfrank, *Fuzzy Control*, vol. 42. New York, NY, USA: Citeseer, 1998.
[28] *Fuzzy Logic Toolbox User's Guide*, MathWorks, Natick, MA, USA, 2006.
[29] H. K. Khalil, *Nonlinear Systems*. London, U.K.: Pearson, 2001.
[30] N. Sun, T. Yang, Y. Fang, Y. Wu, and H. Chen, "Transportation control of double-pendulum cranes with a nonlinear quasi-PID scheme: Design and experiments," *IEEE Trans. Syst., Man, Cybern., Syst.*, vol. 49, no. 7, pp. 1408–1418, Jul. 2019.
[31] T. Yang, N. Sun, H. Chen, and Y. Fang, "Observer-based nonlinear control for tower cranes suffering from uncertain friction and actuator constraints with experimental verification," *IEEE Trans. Ind. Electron.*, early access, May 12, 2020, doi: 10.1109/TIE.2020.2992972.
[32] N. Sun, T. Yang, H. Chen, and Y. Fang, "Dynamic feedback anti-swing control of shipboard cranes without velocity measurement: Theory and hardware experiments," *IEEE Trans. Ind. Informat.*, vol. 15, no. 5, pp. 2879–2891, May 2019.
[33] N. Sun, Y. Fu, T. Yang, J. Zhang, Y. Fang, and X. Xin, "Nonlinear motion control of complicated dual rotary crane systems without velocity feedback: Design, analysis, and hardware experiments," *IEEE Trans. Autom. Sci. Eng.*, vol. 17, no. 2, pp. 1017–1029, Apr. 2020.
[34] K. Liao and Y. Xu, "A robust load frequency control scheme for power systems based on second-order sliding mode and extended disturbance observer," *IEEE Trans. Ind. Informat.*, vol. 14, no. 7, pp. 3076–3086, Jul. 2018.
[35] M. K. Sarkar, A. Dev, P. Asthana, and D. Narzary, "Chattering free robust adaptive integral higher order sliding mode control for load frequency problems in multi-area power systems," *IET Control Theory Appl.*, vol. 12, no. 9, pp. 1216–1227, Jun. 2018.
[36] K. J. Åström and K. Furuta, "Swinging up a pendulum by energy control," *Automatica*, vol. 36, no. 2, pp. 287–295, Feb. 2000.

NGO PHONG NGUYEN received the B.S. degree in mechatronics and the M.S. degree in automation and control engineering from Can Tho University, Vietnam, in 2013 and 2015, respectively. He is currently pursuing the Ph.D. degree with the School of Mechanical, Aerospace and Nuclear Engineering, Ulsan National Institute of Science and Technology (UNIST), Ulsan, South Korea. His current research interests include linear and nonlinear control theories and their application to mechatronic systems.

HYONDONG OH (Senior Member, IEEE) received the B.Sc. and M.Sc. degrees in aerospace engineering from the Korea Advanced Institute of Science and Technology (KAIST), South Korea, in 2004 and 2010, respectively, and the Ph.D. degree in autonomous surveillance and target tracking guidance using multiple UAVs from Cranfield University, U.K., in 2013. He worked as a Lecturer of Autonomous Unmanned Vehicles with Loughborough University, U.K., from 2014 to 2016. He is currently an Associate Professor with the School of Mechanical, Aerospace and Nuclear Engineering, Ulsan National Institute of Science and Technology (UNIST), South Korea. His research interests include autonomy and decision making, cooperative control and path planning, nonlinear guidance and control, and estimation and sensor/information fusion for unmanned systems.

YOONSOO KIM (Member, IEEE) received the B.Eng. degree from Inha University, South Korea, in 1999, the M.Sc. degree from the University of Minnesota, USA, in 2001, and the Ph.D. degree from the University of Washington, USA, in 2004, all in aerospace engineering. He held postdoctoral and senior lecture positions with the University of Leicester, U.K., from 2004 to 2007, and the University of Stellenbosch, South Africa, from 2007 to 2011, respectively. Since 2011, he has been a Faculty Member of the Department of Aerospace and Software Engineering, Gyeongsang National University, South Korea, where he is currently a Professor. His main field of research interest includes distributed control of networked dynamical systems.

JUN MOON (Senior Member, IEEE) received the B.S. degree in electrical and computer engineering and the M.S. degree in electrical engineering from Hanyang University, Seoul, South Korea, in 2006 and 2008, respectively, and the Ph.D. degree in electrical and computer engineering from the University of Illinois at Urbana-Champaign, USA, in 2015. From 2008 to 2011, he was a Researcher with Agency for Defense Development (ADD), South Korea. From February 2016 to February 2019, he was an Assistant Professor with the School of Electrical and Computer Engineering, Ulsan National Institute of Science and Technology (UNIST), South Korea. From February 2019 to August 2020, he was with the School of Electrical and Computer Engineering, University of Seoul, South Korea, as an Assistant Professor and Associate Professor. He is currently an Associate Professor with the Department of Electrical Engineering, Hanyang University, Seoul. His research interests include stochastic optimal control, differential games and estimation, distributed optimal control, and mean field games. He was a recipient of the Fulbright Graduate Study Award, in 2011.

JUN YANG (Senior Member, IEEE) received the B.Sc. degree from the Department of Automatic Control, Northeastern University, Shenyang, China, in 2006, and the Ph.D. degree in control theory and control engineering from the School of Automation, Southeast University, Nanjing, China, in 2011.

He is currently a Senior Lecturer with the Department of Aeronautical and Automotive Engineering, Loughborough University, U.K. His current research interests include disturbance estimation and compensation, advanced control theory, and its application to flight control systems and motion control systems. He received the Premium Award for the best paper of *IET Control Theory and Applications*, in 2017, and the ICI Prize for the best paper of the *Transactions of the Institute of Measurement and Control*, in 2016. He is an Associate Editor of the *Transactions of the Institute of Measurement and Control*.

WEN-HUA CHEN (Fellow, IEEE) received the M.Sc. and Ph.D. degrees from the Department of Automatic Control, Northeast University, China, in 1989 and 1991, respectively. He is currently a Professor of Autonomous Vehicles with the Department of Aeronautical and Automotive Engineering, Loughborough University, U.K. From 1991 to 1996, he was a Lecturer with the Department of Automatic Control, Nanjing University of Aeronautics and Astronautics, China. He held a research position and then a lectureship in control engineering with the Centre for Systems and Control, University of Glasgow, U.K., from 1997 to 2000. He has published three books and 250 articles in journals and conferences. His research interests include the development of advanced control strategies and their applications in aerospace engineering, particularly in unmanned aircraft systems. He is a Fellow of the Institution of Engineering and Technology, and the Institution of Mechanical Engineers.